

# Simulation of the Electrical Resistance Sintering of Hardmetal Powders

Juan Manuel Montes<sup>1</sup>, Francisco J. de la Viña<sup>1</sup>, Íñigo Agote<sup>2</sup>, Thomas Schubert<sup>3</sup>, Francisco G. Cuevas<sup>4\*</sup>, Yadir Torres<sup>1</sup>, José María Gallardo<sup>1</sup>, Jesús Cintas<sup>1</sup>

<sup>1</sup> Department of Materials and Transportation Engineering and Science, Escuela Técnica Superior de Ingeniería, Universidad de Sevilla, Camino de los Descubrimientos s/n. 41092 Sevilla, Spain; jmontes@us.es, fdlavina@us.es, ytorres@us.es, josemar@us.es, jcintas@us.es

<sup>2</sup> Tecnalía Research & Innovation, Industry & Transport Division, Mikeletegi Pasealekua, 2. 20009 San Sebastián, Spain; inigo.agote@tecnalia.com

<sup>3</sup> Fraunhofer Institute for Manufacturing Technology and Advanced Materials, IFAM Winterbergstrasse, 28. 01277 Dresden, Germany; Thomas.Schubert@ifam-dd.fraunhofer.de

<sup>4</sup> Department of Chemical Engineering, Physical Chemistry and Materials Science, Escuela Técnica Superior de Ingeniería. Universidad de Huelva, Campus El Carmen, Avda. Tres de marzo s/n. 21007 Huelva, Spain; fgcuevas@dqcm.uhu.es

\* Correspondence: fgcuevas@dqcm.uhu.es, Tel.: +34 959217448

## Abstract

The simulation of the *Electrical Resistance Sintering* (ERS) of hardmetal powders has been studied. The ERS process can produce a quick consolidation of electrical conductive powders by the simultaneous application of pressure and electrical current. A model of the process has been developed, integrating three actions, namely, thermal, mechanical and electrical, and taking into account the nature of both the powders and the die where powders are placed. The model has been implemented in COMSOL Multiphysics, a finite element commercial program. This paper deals with the model fundamentals and hardmetal particular aspects, such as modelling properties of mixed powders and its thermal behaviour. Other parameters in the model have been tuned to optimally fit the initial experimental data. To check simulation results, measurable parameters have been monitored during experimental tests with WC - 6 wt.% Co. Once the model was completed and put to work, results are discussed.

**Keywords:** modelling and simulation; electrical resistance sintering; powder processing; hardmetal

## 1. Introduction

Although the conventional route of cold pressing and furnace sintering is the most common technology in powder metallurgy (PM) industrial processes, different alternatives have been continuously searched. Grasso et al. [1] reviewed the development of electrical sintering

different modalities. The broad spectra of proposed techniques are known as *field-assisted sintering techniques (FAST)*. Indeed, all those processes are expeditious. However, despite of apparent common aspects of different FAST variants, detailed studies have shown that underlying physical phenomena are quite different.

These techniques use electric currents to activate or improve sintering. In 1906, Lux [2] registered the first patent on powder sintering using direct current. The main purpose of his inventions was the industrial scale production of filaments for incandescent lamps by compacting tungsten or molybdenum particles. In 1913, Weintraub and Rush [3] patented a modified sintering method where electrical current and pressure were combined. The benefits of this method were tested by sintering refractory metals, as well as conductive carbide or nitride powders. In 1933 Taylor [4] described the *Electrical Resistance Sintering (ERS)* process, one of the FAST techniques, and it was around 1955 when Lenel [5] carried out a systematic study. Later, the ERS technique has incorporated different technical variations, such as the use of a resistance welding machine adapted for this process [6]. Essentially, the ERS consists on passing a low-voltage high-intensity alternating current through a powder mass, for a typical period of around 1 s. All over the process, the powder is maintained under pressure in an insulating die. Powder densification occurs in such a short time due to high temperature softening caused by Joule effect heating the powder.

The FAST processes have been commonly approached from an experimental point of view, but not a theoretical one. Nevertheless, SPS (Spark Plasma Sintering), one of the FAST modalities, has received greater attention by researchers in the last two decades, and this has led to a greater theoretical development. Unfortunately, SPS differs from the ERS in two main aspects: SPS has a longer duration (minutes versus seconds) and the SPS dies are electrically conductive. This makes the theoretical developments of SPS not applicable to ERS. Arduous modelling of the effective properties of powder masses is the main reason for the general retard in theoretical studies, i.e., finding equations that adequately describe the thermal, electrical and densification behaviours is not an easy task.

A detailed list of the theoretical and experimental works dealing with the FAST processes can be found in the review of the electric current activated sintering techniques by Orrù et al. [7] and Munir et al. [8]. A detailed study of the scalability of the SPS technique was carried out by Olevsky et al. [9], including a finite element analysis [10]. Regarding the ERS process, a complete one-dimensional model was developed by Montes et al. [11].

Advantages of developing an ERS theoretical model are outstanding because there is no a simple way to relate sintering conditions and final results. For instance, it could be thought that, due to ceramic die durability issues, a desirable high pressure would not be attainable. But in ERS the real reason is that higher pressure values do not necessarily lead to higher densities in the final compact. Indeed, the low electrical resistivity of a highly compacted powder mass will result in a low energy dissipated by Joule effect. Moreover, closed porosity inside a tightly pressed compact will eventually release gasses during heating, avoiding densification or even producing the expansion of the compact, despite of the applied pressure. Therefore, only the appropriate selection of the process parameters drives to reasonable densification rates, avoiding an excessive grain growth (in general detrimental for mechanical properties) and allowing for the release of gasses. Additionally, a theoretical model giving exact predictions of temperatures, thermal gradients, movements in the ERS equipment parts will help in die and other parts design.

An advanced ERS simulator would allow the prediction of temperature and porosity inside the powder aggregate, which are difficult to measure experimentally. It could also help in choosing the current, processing time, external pressure, and even the optimum die materials. Such a model could establish the basis for a possible industrial-scale production.

In this work, a finite elements implementation of a model to describe the ERS process, which is similar to that partially described in [11], is reported and applied to not elemental powders. The selected powder is a mixture of WC and Co particles, in the frequent commercial proportion WC - 6 wt.% Co.

The application of the ERS process to hardmetal powders is not a novelty. Taylor's pioneering work [4] already used powders of this nature. From then until now, the fact that this material and its applications can take advantage of the ERS process has not changed.

## **2. Experimental set-up**

An adapted resistance welding machine (Beta 214 MF, Serra Soldadura S.A., Barcelona, Spain) with medium frequency technology (1000 Hz) was used for the experiences. The controlled variable in the system is the intensity of a direct (rectified alternating) current. The system to be modelled consists of a die, and electrodes 12 mm in nominal diameter; the latter conveniently divided in punches and wafers to implement the process. The metallic powder mass was contained between the two 5 mm height wafers, and enclosed into the electrically insulating die (a ceramic tube 3 mm in thickness and 50 mm in height). A metallic (steel) hoop with 30 mm

of external diameter surrounds the ceramic die to help improving its mechanical strength. The whole system is schematically shown in Fig. 1.

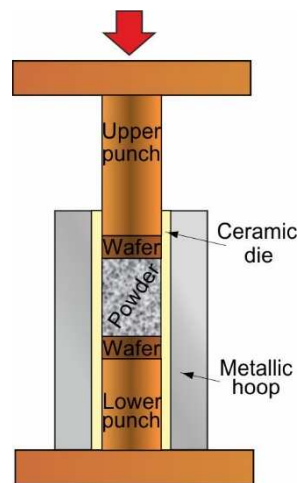


**Fig. 1** Electrical resistance sintering scheme. The punches are refrigerated at constant temperature.

Punches and their bases (98.9%Cu-1%Cr-0.1%Zr) and wafers (75.3%W-24.6%Cu) must have low thermal but high electrical conductivity. High thermal conductivity punches/wafers would increase heat losses preventing sufficiently high temperatures in the powder mass. The requirement of high electrical conductivity is related to the limited voltage that the equipment can apply (usually less than 10 V). High electrical resistance electrodes/wafer would decrease the electrical current flowing through the system and, hence, the Joule effect heating of the powder mass.

The model resembles the typical experimental sequence of the ERS process. It begins with a *cold compaction stage* during which no electrical current passes through the powder, but constant pressure (100 or 250 MPa) is applied. Once finished, a *hot pressing or heating stage* begins, with the pressure kept constant and the system driven by the electrical current of a fixed value, respectively). Finally, the process ends with the *cooling stage*, in which the pressure is maintained for 300 ms, but no current acts, so that the compact is cooled under pressure.

On the other hand, the system is monitored to precisely know the position of the upper electrode at any time. After any experiment, the final height of the compact is measured, allowing to calculate the precise height of the powder column in every instant. Mean porosity of the powder mass can be computed from its volume throughout the experiment. This is carried out, according to the definition of the density of the powder column, by:

$$\Theta = 1 - \frac{M}{H \cdot S_N \cdot \gamma_m} \quad (1)$$

where  $\Theta$  is the overall porosity of the powder column for a particular moment,  $M$  the powder mass,  $H$  is the height of the powder column for such moment,  $S_N$  the powder column section area, and  $\gamma_m$  is the absolute or bulk density of the WC-6Co powders. Tools thermal expansion was not taken into account for this computation.

In addition, the current intensity, voltage between the bedplates of the electrodes, and the applied load through the punches are monitored for every moment of the process, therefore having precise data to check results of the electrical and mechanical problem of the model. On the other hand, temperature is not experimentally measured, therefore not being possible a comparison between experimental and modelled values.

Finally, it is compulsory to carry on a previous characterization of the mechanical and electrical behaviour of the powders. The compressibility curve of the powders due to cold pressing under an increasing load was studied according to the MPIF Standards [12]. On the other hand, the resistivity of the powder column for different porosities was recorded by measuring the voltage drop between the electrodes for a known intensity. Once known the electrical resistance and taking into account the geometry of the system and the properties of the punches, the resistivity of the powder column was finally computed.

### 3. Brief description of the model

The modelling of the ERS process requires the study of the transfer of thermal energy generated by the passage of electric current through the system, as well as the problem associated with the densification of the system. The powder between the electrodes may densify by the effect of the applied pressure and high temperature softening. At the same time, electrical, thermal and mechanical properties of the powder depend simultaneously on porosity and temperature. As a consequence, the problem solving of porosity reduction is affected by a strong coupling between two physical problems: heat transfer and mechanical behaviour. According to this, variables such as the evolution and distribution of temperatures and porosities, and other such as the electrical resistance, specific thermal energy generated, etc. must be known at any instant of the process to complete the model resolution.

The most complex problem arises during current passing stage, when two coupled sub-problems, mechanical and thermal, have to be considered. It should be noted that although a

constant current intensity is applied during the process, there is indeed an electrical problem associated with the experiments. The porosity variation of the powder column makes the electrical resistance of the powder column to change. This certainly will derive in a thermal problem because of the change of the Joule effect in the powder column.

The whole model will be solved by COMSOL finite elements program, considering a 2D axial symmetry according to the geometry described in Fig. 1.

### 3.1. The mechanical problem

During the cold pressing stage, powder is subjected to a nominal pressure  $P_N$ , and its porosity is reduced from the tap porosity  $\Theta_M$  (calculated according to the MPIF Standards [13]) to the initial value during current passing stage,  $\Theta_0$ . This initial value can be modelled by the Secondi equation [14], expressed in terms of porosity as:

$$\Theta_0 = \Theta_\infty + (\Theta_M - \Theta_\infty) \exp\left(-\left(P_N/a\right)^b\right) \quad (2)$$

The values of the parameters  $\Theta_\infty$ ,  $a$  and  $b$  are obtained by least square regression fitting of the experimental powder compressibility curve values (obtained according to MPIF Standards [12]) to the Secondi expression.

During the heating and cooling stages, the porosity of each finite element at the domain of the powder mass is further reduced according to the following law proposed by Montes et al. [15]:

$$\frac{\dot{\theta}}{\theta} = -\dot{\varepsilon}_c \quad (3a)$$

with

$$\dot{\varepsilon}_c = \frac{A_c}{T} \cdot \left( \frac{\sigma_{eq}}{E_m} \cdot \frac{\sqrt{\theta/\Theta_M}}{1-\theta/\Theta_M} \right)^{n_c} \cdot \exp\left(-\frac{Q_c}{RT}\right) \quad (3b)$$

where  $\theta$  is de local porosity,  $T$  the local absolute temperature,  $\dot{\varepsilon}_c$  the local true strain rate, and  $\sigma_{eq}$  is the local equivalent stress (the Von Misses tension) responsible of the powder deformation and densification, and depending on the value of  $P_N$ . (By ‘local’ we mean, obviously, that these properties vary from one point in the system to another.) Computing the

exact value of local  $\sigma_{eq}$  is automatically made by COMSOL taking into account the boundary condition imposed by the pressure  $P_N$  applied by the upper punch. Regarding parameters of the fully dense material,  $E_m$  is the Young modulus at room temperature (a fix value, only for the purpose of renormalization),  $A_c$  is the pre-exponential factor in the Norton creep law, and  $n_c$  and  $Q_c$  are the creep exponent and the creep activation energy, respectively.  $R$  the ideal gas constant.

The initial condition for the porosity, at the start of the heating stage, for the whole volume occupied by the powder is:

$$\theta(t=t_0) = \Theta_0 \quad (3c)$$

It is worth noting that the model does not consider the inherent densification of a conventional sintering process, because of the very short processing times which practically inhibit the atomic diffusion processes. This would be not the case in other FAST processes, for instance SPS, but it is a valid consideration in the ERS process.

### 3.2. The thermal problem

When the powder mass is traversed by a current intensity  $I$ , the temperature throughout the system is computed by solving the following thermal problem, as proposed by Haberman [16]:

$$\frac{\partial}{\partial t}(\gamma c T) = \vec{\nabla} \cdot (k \vec{\nabla} T) + \frac{I^2 \rho}{S_N^2} \quad (4a)$$

where the coefficients  $\gamma$ ,  $c$ ,  $k$  and  $\rho$  (density, specific heat, thermal conductivity and electrical resistivity respectively) are functions depending on the considered position of the system and the temperature. The problem has to be completed with the initial condition:

$$T(\vec{r}, 0) = T_0, \text{ in all the system} \quad (4b)$$

and the following boundary condition, related to the cooling of electrodes:

$$T(t) = T_c, \text{ at the electrode bases at any time} \quad (4c)$$

Finally, the system parts in contact with air are considered to cool down according to an air Newton cooling law, directly implemented by COMSOL.

### 3.3. Materials properties

Die, punches and powder properties are considered to be temperature dependent. Specific heats of the phase transformations are also taken into account in the case of the powder. The thermal dependences of the components properties can be found listed in specialized literature, such as Gale and Totemeier [17] and Pierson [18]. It is worth noting that, surprisingly, the element Co and the compound WC are not perfectly characterized at high temperatures, and it has been necessary to extrapolate some data.

The powder mass properties have an additional dependence: the porosity degree. The apparent or effective properties (density,  $\gamma$ ; specific heat,  $c$ ; electrical resistivity,  $\rho$ ; and thermal conductivity,  $k$ ) of any volume of the powder mass depend on its porosity ( $\theta$ ) as described by Montes et al. [11]:

$$\gamma = \gamma_m (1 - \theta) \quad (5a)$$

$$c = c_m \quad (5b)$$

$$\rho = \rho_m \left[ (1 - \theta / \Theta_M)^{-\frac{3}{2}} + \frac{6\alpha}{\pi} (1 - \theta / \Theta_M)^{-\frac{1}{2}} \right] \quad (5c)$$

$$\text{with } \alpha = \left( \frac{\rho_x \delta}{\rho_m r} \right) \exp(-m_d (1 - \theta / \Theta_M)^{n_d}) \quad (5d)$$

$$k = k_m (1 - \theta / \Theta_M)^{\frac{3}{2}} \quad (5e)$$

where  $\gamma_m$ ,  $c_m$ ,  $\rho_m$ , and  $k_m$  are the respective properties of the bulk material, and  $\rho_x$  is the electrical resistivity of the oxide covering the powder particles. The powder shape and behaviour is characterised by the parameters  $r$  (the mean radius of the particles),  $\delta$  (the mean thickness of the oxide layer) and  $\Theta_M$  (the tap porosity). The oxide descaling process of the powder particles is modelled by the dimensionless parameters  $m_d$  and  $n_d$ .

The electrical resistivity of the cobalt oxide, which is supposed to be the most influent specie, and the parameters describing its thermal dependence, are given by the well-known expression by Kingery et al. [19]:

$$\rho_x(T) = A_x \exp(E_x / (2k_B T)) \quad (6)$$

where  $A_x$  is a pre-exponential factor,  $E_x$  is the band-gap energy and  $k_B$  is the Boltzmann constant.

An additional problem occurs when the type of powder is not elementary, as is now the case. Appropriate mixing laws are necessary to model the system. Considering a mixture of two phases, being  $f_i$  and  $\phi_i$  the mass and volume fractions of the phases, the properties of the mixture, can be calculated as

$$\gamma_m = \left[ \sum_{i=1}^n f_i (\gamma_{m_i})^{-1} \right]^{-1} \quad (7a)$$

$$c_m = \sum_{i=1}^n f_i \left( c_i + \sum_j G_i^{T_j} L_{m_i}^j \right) \quad (7b)$$

$$\kappa_m = \sum_{i=1}^n \phi_i \kappa_{m_i} \quad (7c)$$

$$\rho_m = \left[ \sum_{i=1}^n \phi_i (\rho_{m_i})^{-1} \right]^{-1} \quad (7d)$$

where  $L_{m_i}^j$  is the  $j$ -th latent heat of the component  $i$ , which is released/absorbed at temperature  $T_j$ . The function  $G_i^{T_j}$  is the Gaussian function described as:

$$G_i^{T_j} = \frac{1}{\varepsilon \sqrt{\pi}} \exp \left( - \left( \frac{T - T_j}{\varepsilon} \right)^2 \right) \quad (7e)$$

where  $T_j$  is the temperature of the phase transition and  $\varepsilon$  is a small quantity that represents the semi-width of the curve.

The use of the mixture laws requires knowing the value of the considered property for all the components of the mixture at the same temperature. Usually, the properties are not assessed at the same temperature in the bibliography, and the additional problem of interpolating data

clouds has to be considered. The interpolation technique based on cubic splines was used in this work.

#### 4. Implementation with COMSOL Multiphysics 5.0

When working with finite elements, fixed meshes cannot accurately reproduce a deforming geometry. In this work, adaptive meshes are required due to the powder densification. In COMSOL, an adaptive mesh is automatically created in solid mechanics when the nonlinearity geometry option is chosen. However, an adaptive mesh must be introduced independently in the thermal and electrical problems.

In this work, the geometry is defined as two assembled domains, one with an adaptive mesh and the other with a fixed mesh. The domain constituted by moving parts of the system during the experiences corresponds to the adaptive mesh (upper electrode and wafer, and powder). The domain whose geometry is fixed corresponds to the fixed mesh (die, steel wrapping, lower electrode and wafer). Fig. 2 shows the two aforementioned domains.

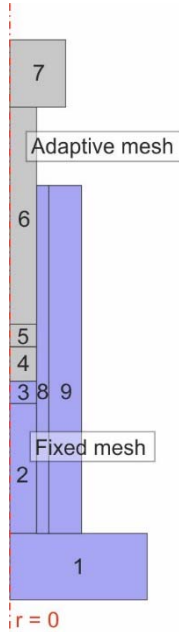


**Fig. 2** System showing the two constituting domains described with adaptive and fixed meshes. Parts numbered with 1, 2, 6 and 7 represent the punches, 3 and 5 the wafers, 8 and 9 the die and hoop and 4 the powder mass.

The only condition required in the fixed mesh is that the mesh works with fixed elements. For the adaptive mesh it is necessary to set the displacements of all boundaries with respect to the fixed mesh. In the case of the upper punch and wafer, only vertical movements of the mesh

are allowed. Two kinds of finite elements have been used: triangular and rectangular. In the last option to take advantage of the system axial symmetry.

The procedure followed in COMSOL to predict the theoretical behaviour starts with the knowledge of the global porosity in the powder in every instant. To make this, the porosity variation of each finite element is computed from Eqs. (2) for each instant. However, the new value of the porosity does not directly change the volume of the finite element, this is something that COMSOL cannot directly control. (The models available in COMSOL to deal with non-linear strains are restricted to smaller strains than those present in the problem to be solved.) To overcome this problem, first, the overall porosity ( $\Theta$ ) is calculated by the integral average in the compact. On the other hand, the new powder column height is computed from Eq. (1), relating the height of the powder column ( $H$ ) to the overall porosity of the powder. Once known the new powder column height and the powder/electrode interface has been relocated, the domain mesh is automatically deformed (and regenerated) by COMSOL.

Also, solid mechanics, heat transfer and electric current moduli ('physics' in COMSOL terminology) must be used. Each one of these 'physics' is related with the others. Furthermore, other 'physics' must be taken into account, the differential equations solving module for the calculation of the porosity. It is important to emphasize that the studied problem is an axial symmetry 2D problem, and all the 'physics' take advantage of this. Of course, it is required to impose continuity conditions for the studied properties in order to ensure that all solved variables are continuous in the entire model.

In order to obtain a reliable mesh, the number of finite elements was varied (mesh sensitivity analysis) in such a way that the relative discrepancies of porosity and average temperature in the final instant of the ERS process were less than 1% among different simulations with small differences in the number of finite elements.

On the other hand, a maximum time step (the difference between two simulated instants) was allowed to ensure that relative discrepancies were less than 1%. Likewise, Backward Differentiation Formulas (BDF) were enabled, automatically reducing the time step to force a better convergence in case of contingencies. These methods (a family of implicit methods) are linear multistep methods that approximate the time derivatives using information from already computed times, thereby increasing the accuracy of the approximation. It has been found that the maximum time step does not alter, to a large extent, the final results obtained, as long as it is lower than 5 milliseconds. With longer time steps, the simulation did not converge.

The relative and absolute tolerances for most dependent variables (voltage, porosity and displacements) were set to 0.001, and in the case of the temperature both tolerances could be increased to 0.01. Increased tolerances for other variables lead to divergence in some situations.

Finally, Newton's method for solving each independent problem has been chosen, due to their clear non-linear behaviour.

With the aforementioned conditions, the computational time of a complete simulation is of the order of one hour.

## 5. Experimental results and simulations

### 5.1. Materials and experimental conditions

Concerning the materials used to validate the model, a mixture of ultrafine WC (grain size of  $262 \pm 77$  nm) and Co, from Kyocera Unimerco (Sunds, Denmark), was used. This powder mix forms spherical agglomerates after being degassed and presintered, with a mean particle size of  $141 \mu\text{m}$ . SEM micrographs of the powder are shown in Fig. 3.

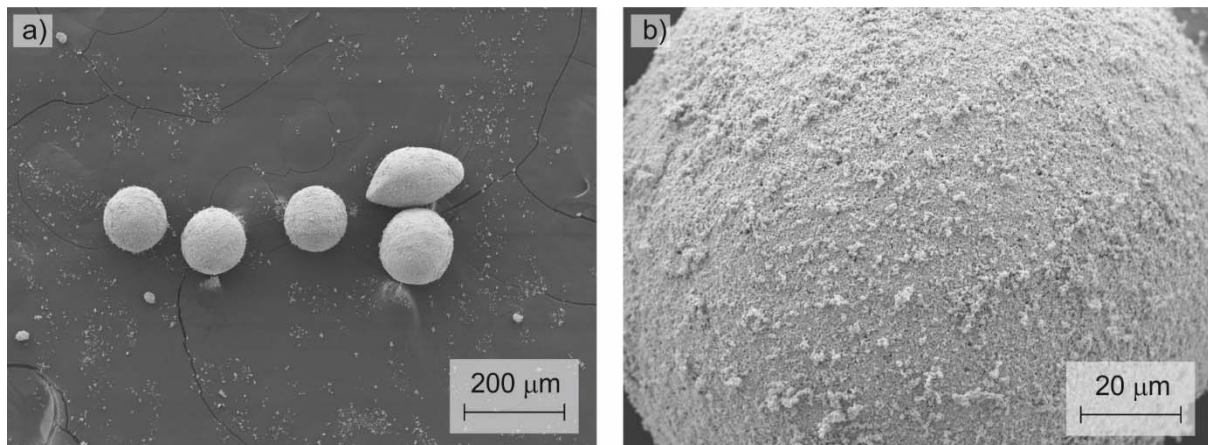


**Fig. 3** a) SEM image of the WC - 6 wt.% Co powder from Kyocera Unimerco, used in ERS experiences, b) higher magnification image.

A powder mass of 6.5 g is poured into the die and vibrated up to reach its tap porosity [13]. This constitutes the initial situation of the powder for the experiments. A value of  $\Theta_M = 0.7$  was experimentally obtained. Both alumina and sialon dies were used. All the experiments, but those in which these two materials are compared, were carried out with the alumina die.

During experiment, and also as inputs in the simulation processes, several parameters have to be selected. Thus, the nominal pressure  $P_N$  has been chosen between 100 and 250 MPa, the current intensity  $I$  among 5, 5.5, 6.5, 9 and 14 kA, the cold pressing stage always lasted 1000 ms,

the heating stage varied among 300, 400, 500 and 1000 ms, and the final cooling was always of 300 ms.

## 5.2. Strategy of validation

The equations in the model have to be fed with the involved parameters values. Some of these values are easily found in the literature, as is the case of the thermal dependences [17, 18]. Others required searching in specialized literature. Thus,  $Q_c$  in Eq. (3b) is considered to be 470 kJ/mol according to Frost and Ashby [20];  $\delta$  in Eq. (5d) is fixed to 4.5 nm according to Evans [21], and  $A_x$  and  $E_x$  in Eq. (6) take the values  $A_x = 3.59 \cdot 10^{-11} \Omega \cdot \text{m}$  and  $E_x = 144552 \text{ J/mol}$  (Evans [21] and Tsuda et al. [22]). The values of the parameters  $m_d$  and  $n_d$  in Eq. (5d) were obtained by fitting the experimental resistivity-porosity curve of the powder. The resultant values were  $m_d = 129.502$  and  $n_d = 0.0638$ . Moreover, the values of the parameters in the Secondi equation (obtained by fitting the experimental compressibility curve) were  $\Theta_\infty = 0.001$ ,  $a = 756.33 \text{ MPa}$  and  $b = 1.1728$ .

On the other hand, the model considers two fitting parameters, whose values are difficult to measure and know. These parameters are  $A_c$  and  $n_c$ , (Eq. (3b)), which control the creep densification rate. Their values are chosen by the COMSOL optimization modulus, by comparing the simulated and experimental evolution of the compact global porosity during the initial ERS process used to define the whole model. Once  $A_c$  and  $n_c$  are fixed from this particular experiment, they will be considered constant for any other experiments carried out with the same powder under different processing conditions (different pressure, current dwelling time and/or current intensity, and die material).

Fig. 4 shows (upper curves) the fitting obtained between the global porosity experimental curve, used as objective curve (solid line, obtained for 100 MPa, 5.5 kA and 400 ms of heating), and the theoretical one fitted with the best values of  $A_c$  and  $n_c$  optimized by COMSOL (dotted line).

The optimum values of the fitting parameters previously found ( $A_c = 32$  and  $n_c = 3.2$ ) can now be used to predict the evolution of any other parameter in the system, e.g., the porosity in an experiment where the intensity changes to 6.5 kA. The result is shown in Fig. 4 (lower curves), where fitting is still reasonably good with the experimental curve (solid curve).

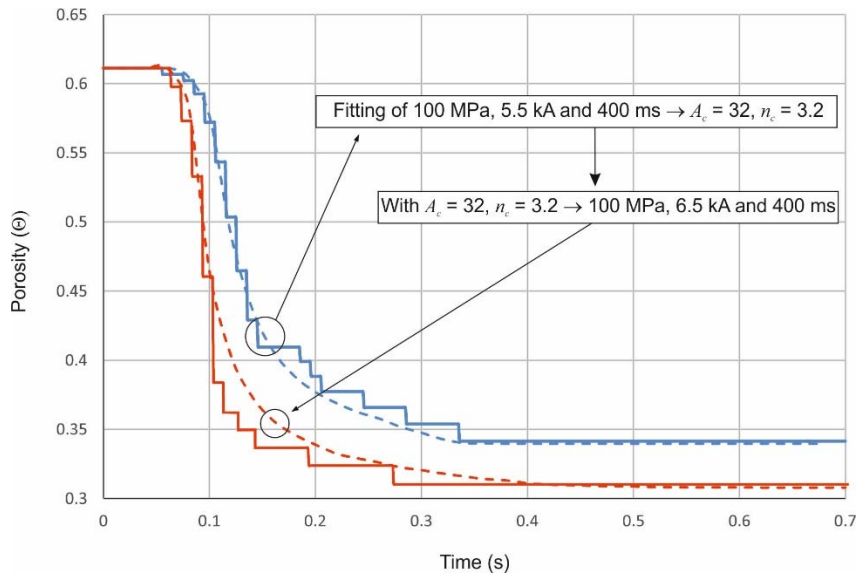


**Fig. 4** Experimental (solid) and simulated (dotted) curves obtained for ERS experiences with pressure of 100 MPa, and intensity of 5.5 kA (or 6.5 kA) applied for 400 ms. (The stepped shape of the experimental curve is a consequence of the noise reduction function of the displacement sensor.)

As a final product of the simulation, several outputs can be obtained. Fig. 5 shows the porosity distribution inside a compact and the temperature distribution at the whole system, in the final instant of an experience carried out with 100 MPa and 5.5 kA, for 400 ms of heating time. The porosity distribution shows a densified core and an outer porous layer, as experimentally confirmed in Fig. 5c. Regarding the temperature, predictions cannot be experimentally confirmed, but the simulation can help understanding the obtained results in the experiences.

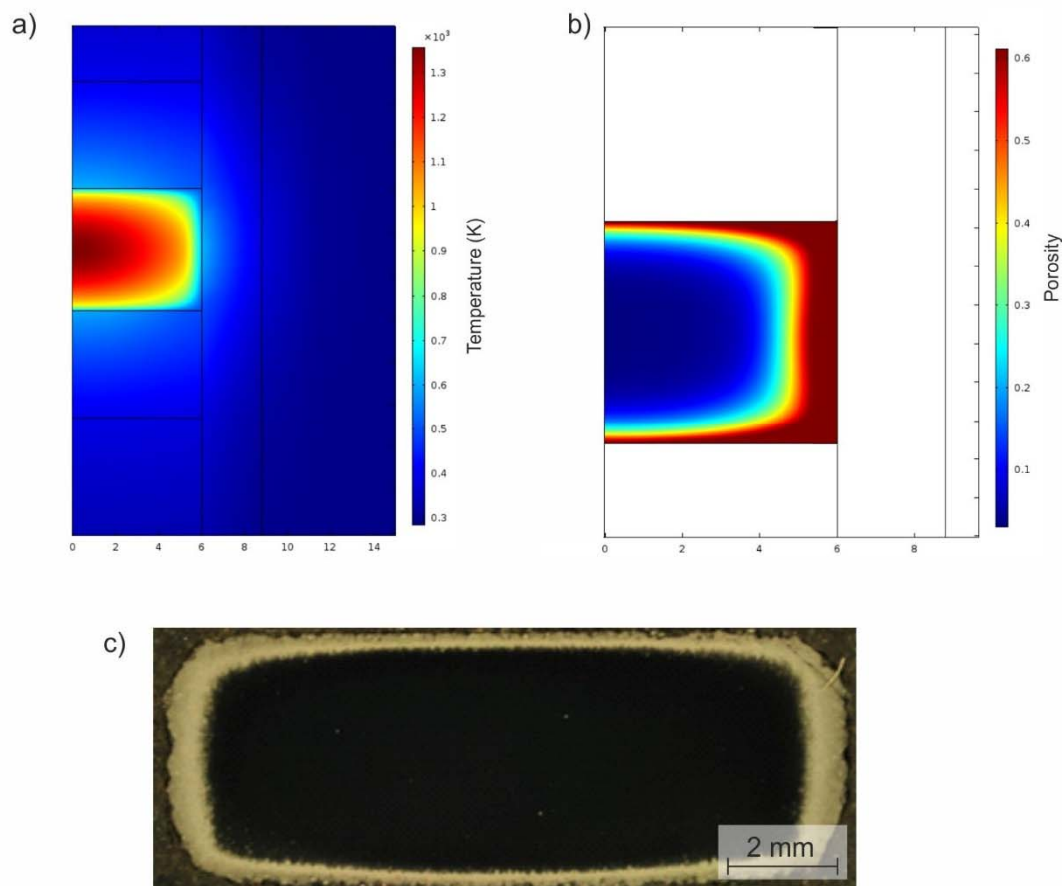


**Fig. 5** Simulation result of (a) system temperature distribution and (b) the compact porosity, for the final instant of an experience with 100 MPa of pressure, intensity of 5.5 kA and heating stage of 400 ms. In (c), a micrograph of a diametrical section of a compact (12 mm diameter), consolidated with these same conditions, can be observed, showing a porous periphery and a denser core.

This information is only accessible with the model prediction, but not in an experimental way. In the same way, it is possible to carry out virtual experiments in order to verify the influence that the different process parameters have on the final results. Some of these parameters will be studied in the following sections.

### 5.3. Influence of the heating time

It is interesting to compare the mean temperature and mean porosity evolution obtained after different heating times (e.g., 300, 500 and 1000 ms) while maintaining constant the current intensity and pressure (e.g., 9 kA and 100 MPa). The mean temperature and mean porosity are calculated at each instant of time, averaging integrally in the domain of the powder mass each variable.

As shown in Fig. 6, once heating starts, the maximum temperature is reached in about 100 ms, although the porosity decrease is much slower, needing more than 400 ms to approach its final value.

It is also observed that the maximum reached temperatures remain virtually constant for different heating times, which implies that the final porosities do not vary significantly.

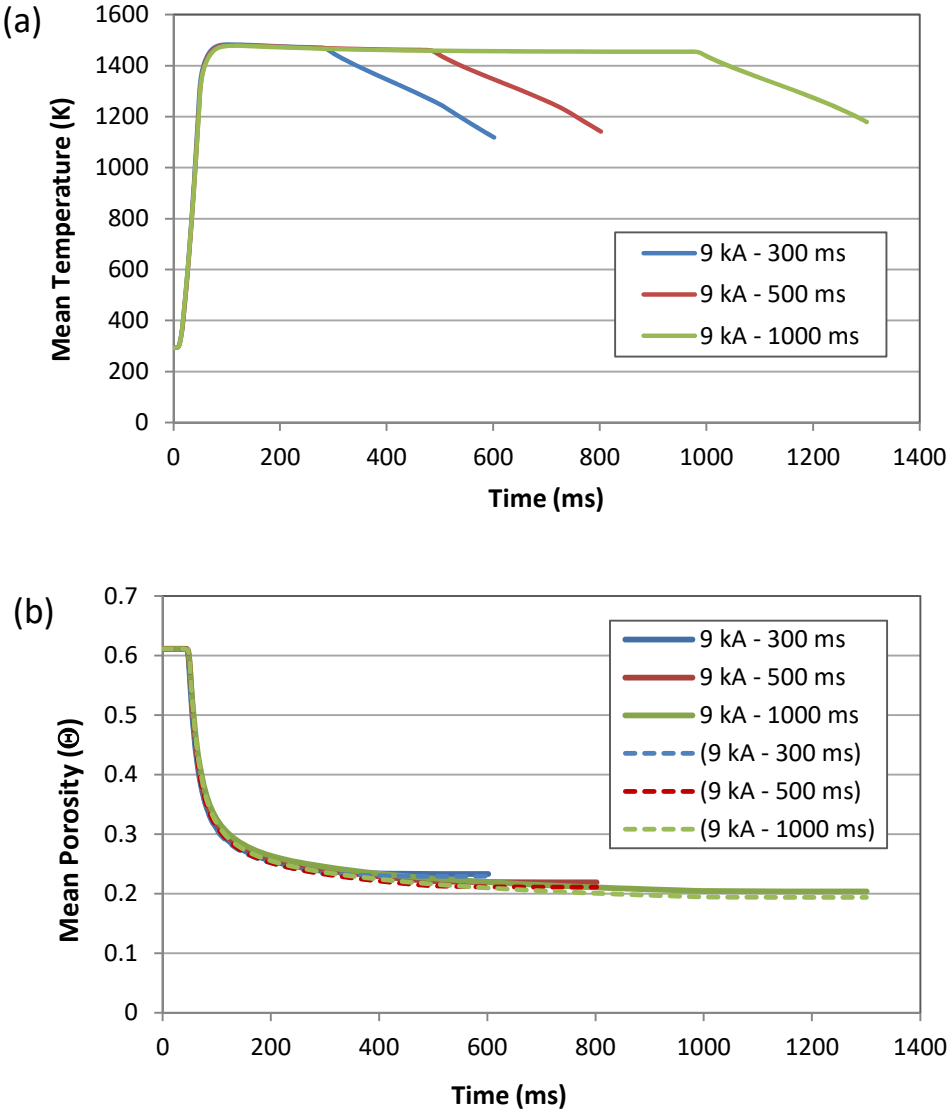


**Fig. 6** Evolution of (a) the mean temperature and (b) mean porosity for different heating times. The solid lines correspond to the simulator predictions; the dashed lines are obtained by processing and smoothing the recorded data.

Predictions about the evolution of the mean temperature cannot be experimentally contrasted, in comparison to those corresponding to the mean porosity that can be easily contrasted. As can be seen in Fig. 6b, simulations are in good agreement with experimentally

obtained results, with the final porosity around 20% in all cases, thus confirming the low incidence of the heating time. The good agreement of these predictions gives some confidence about the temperature predictions offered by the simulator.

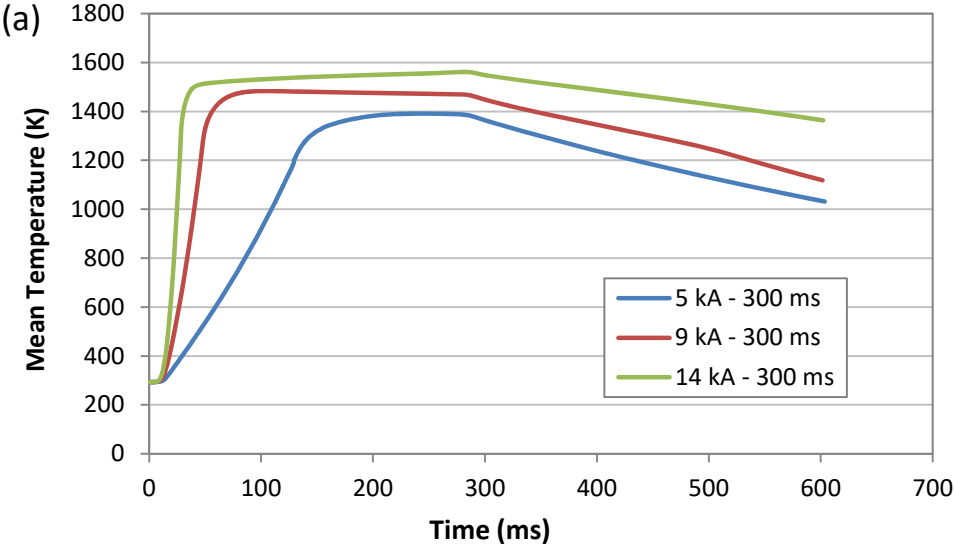
### 5.4. Influence of the current intensity

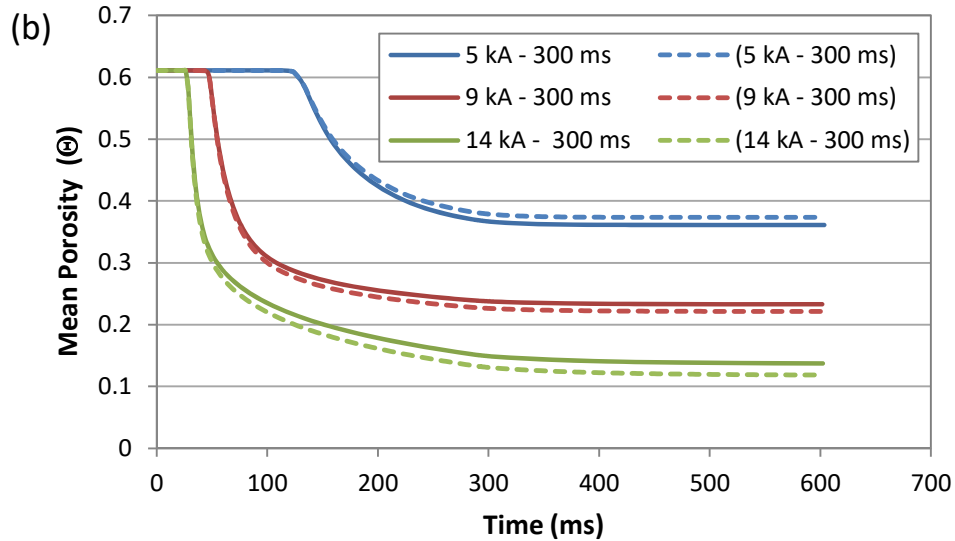
The effect of the current intensity has been checked by comparing the mean temperature and porosity evolution for different values of the heating intensity (5, 9 and 14 kA), while maintaining the same heating time of 300 ms and applied pressure of 100 MPa.

Fig. 7a shows that the higher the intensity, the higher the temperature increase rate and maximum temperature reached. On the other hand, it is easy to see that higher intensities make the porosity to start changing earlier. As a consequence of the higher temperature, greater softening of the powder and greater densification is reached.

It is also observed how, contrarily to the influence of heating time, the final porosity is markedly reduced by increasing the current circulating through the powder mass, making possible to obtain more densified pieces.

Porosity predictions have again been corroborated by comparison with experimentally acquired curves.



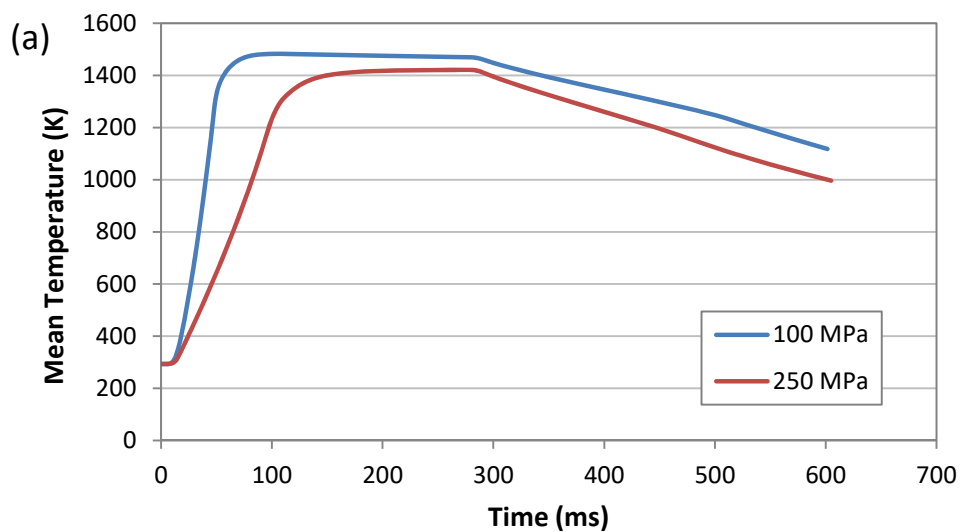


**Fig. 7** Evolution of: (a) the mean temperature and (b) mean porosity for different current intensities. The solid lines correspond to the simulator predictions; the dashed lines are obtained by processing and smoothing the recorded data.

### 5.5. Influence of the applied pressure

The evolution of the mean temperature and mean porosity for different applied pressures (100 and 250 MPa) are now compared. This is done for a heating intensity of 9 kA and a heating time of 300 ms.

As can be seen in Fig. 8, when the pressure is increased, the mean temperature of the powder mass decreases and, therefore, the final porosity values are slightly higher.



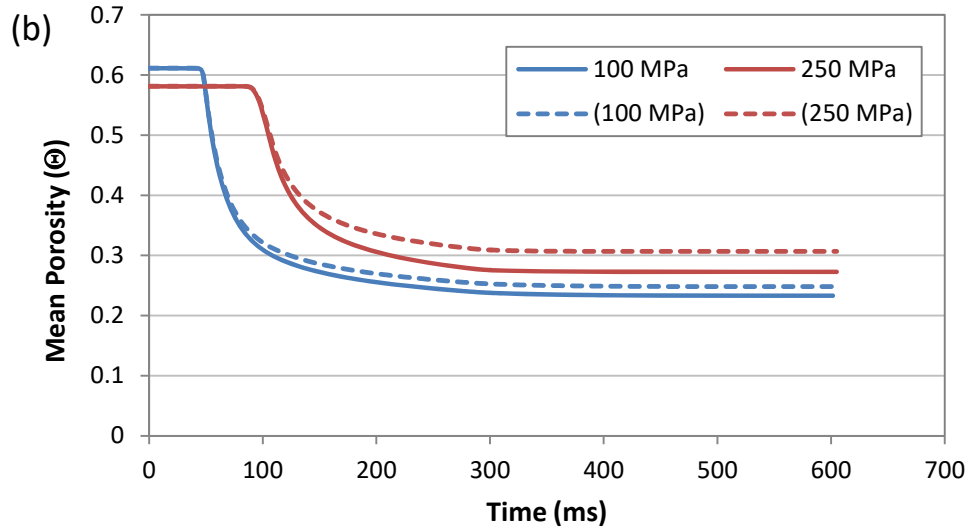


**Fig. 8** Evolution of: (a) the mean temperature and (b) mean porosity, for different values of the pressure. The solid lines correspond to the simulator predictions; the dashed lines are obtained by processing and smoothing the recorded data.

Again, the mean temperature evolution prediction is not contrastable with experimental data. This is only possible for the porosity evolution, as shown in Fig. 8b. The concordance is better for the 100 MPa experience. However, the most important fact is that both experimental and theoretical curves are in agreement in that the experience with 250 MPa results in a higher final porosity. Thus, higher pressures result in lower porosities after the cold compaction stage, but this is counterproductive for subsequent densification during the heating stage. The lower porosity at the beginning of this stage means that the resistivity of the powder mass is lower and, therefore, the thermal energy released by the Joule effect for a particular current intensity will also be lower. Thus, contrarily to expected, higher pressures result in lower densification, i.e., higher final porosities, which is not a priori obvious.

An additional detail that can be seen in Fig. 8b is that the prediction for 250 MPa is worse than that of 100 MPa. This is a logical consequence of the fact that the parameters  $A_c$  and  $n_c$  were optimized for a target curve obtained with an experience with 100 MPa.

## 5.6. Influence of the die material

The evolution of the powder mass mean temperature and mean porosity is now compared when using two different die ceramic materials, alumina and sialon. The arbitrarily chosen test conditions were: current intensity of 10.5 kA, heating time of 400 ms and pressure of 100 MPa.

The evolution of the mean temperature and mean porosity obtained with simulations, and experimentally confirmed for the porosity, for the two materials are shown in Fig. 9.

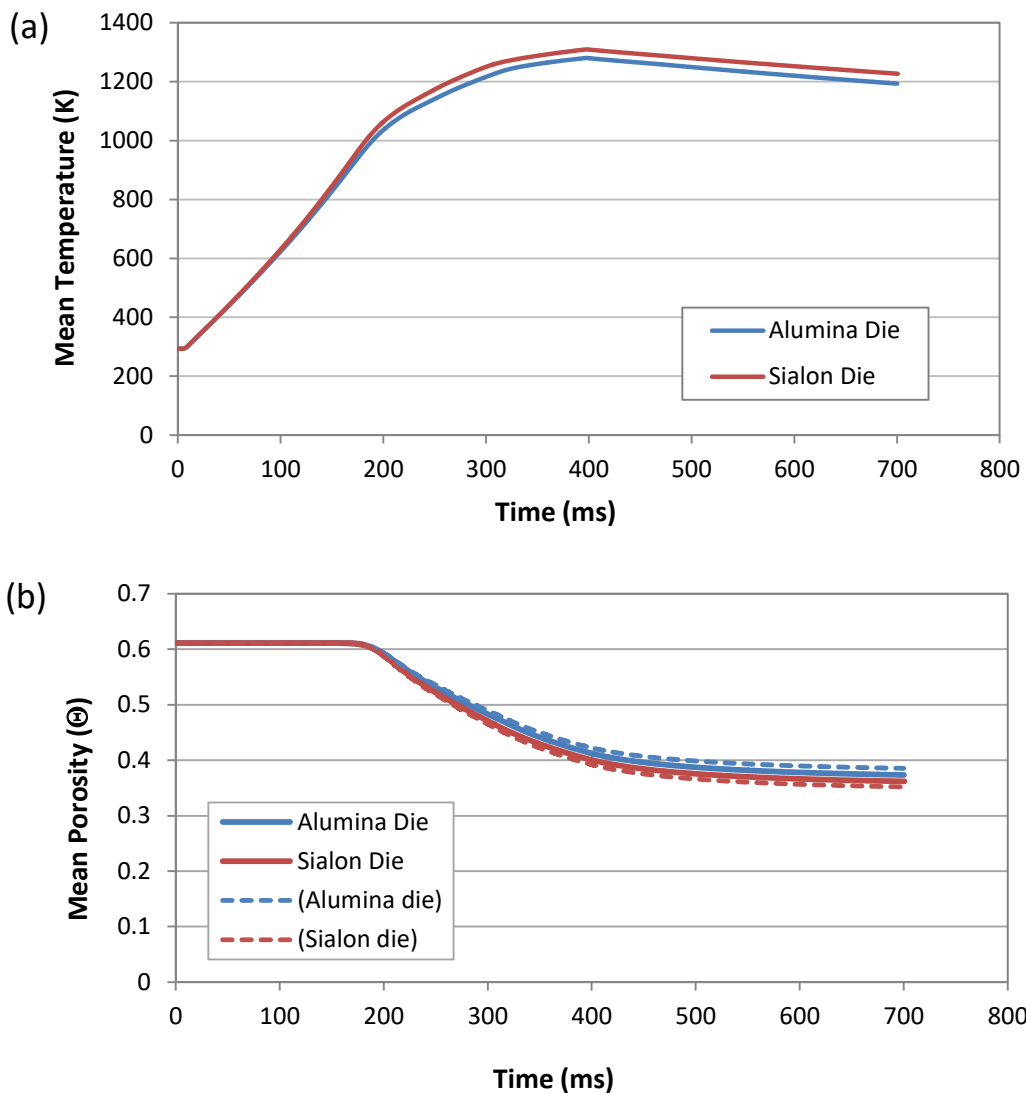


**Fig. 9** Evolution of: (a) the mean temperature and (b) mean porosity, for different die materials. The solid lines correspond to the simulator predictions; the dashed lines are obtained by processing and smoothing the recorded data

Because sialon is worse as a thermal conductor than alumina, heat losses through sialon die walls in contact with powders are lower. It is therefore clear that the mean temperature for the sialon die (as shown in Fig. 9a) is always slightly higher. In the same sense, it is understood that the mean porosity is always somewhat lower for sialon (Fig. 9b). These differences are clear at high temperatures, with the curves following an almost parallel behavior, but not great differences are observed at the beginning of the experience.

On the other hand, the choice of one or other material does not change the instant in which porosity begins to fall, nor does the instant in which the maximum temperature value is reached.

## **6. Model limitations and future work**

The previous results show that the developed model and simulations reasonably agree with the experimentally measured results. It also reinforces the validity of the model and simulations for those conditions that cannot be experimentally validated. Nevertheless, some discrepancies are observed between predictions and experiments. Several reasons could be considered. Regarding experimental aspects, it is assumed that the porosity reaches a uniform value all throughout the powder mass at the end of the cold compaction stage (Eq. (3c)). This is known to be untrue, and it is a consequence of the initial porosity distribution despite powders were always vibrated into the die, and also of the effect of the uniaxial compression. The confinement of gasses that could appear during powder heating (although powder was previously degassed to avoid this problem) has neither been considered. It is also believed that the considered value of the tap porosity could not be as precise as desired. The spherical agglomerates of WC-Co are not completely dense but constituted by particles stuck to each other.

Finally, despite the aforementioned limitations, the model is considered to generate more than acceptable simulations. It can be however improved, a logical extension of this work would be to deal with compacts with more complicated geometries (for instance, without revolution symmetry).

## **7. Conclusions**

The ERS process applied to hardmetal powders has been successfully modelled and simulated using COMSOL Multiphysics. This modelling takes into account plastic and creep densification and solves the mechanical-thermal-electrical coupling that characterizes the process. The simulation results of the ERS process bring about a larger densification in the core than at the outer surface of the powder compact, as confirmed by experiments. The good concordance between predictions and experimentally recorded global porosity curves allows to be confident regarding predictions on temperature distribution, as well as mean temperature evolution. Also, it is acceptable as the model supposes, that heat-assisted creep flow is the main responsible for the densification.

Results obtained for the different tested and simulated conditions, indicate that the increase in heating time does not guarantee to obtain lower porosities; nor does the increase in pressure. The best choice to attain a greater densification is to increase the intensity current. The effect of the die material has also been correctly predicted by the model.

## Acknowledgments

The authors are grateful to EU for funding this research within the framework of the EU 7<sup>th</sup> Framework FoF.NMP.2013-10 608729 EFFIPRO Project. The authors also wish to thank the technician Raquel Astacio (University of Seville) for experimental assistance.

## Compliance with Ethical Standards

Conflict of interests: The authors declare that they have no conflict of interest.

## References

- [1] Grasso S, Sakka Y, Maizza G (2009) Electric current activated/assisted sintering (ECAS): a review of patents 1906–2008. *Sci. Technol. Adv. Mater.* 10(5):1-24.
- [2] Lux J (1906) Improved manufacture of electric incandescent lamp filaments from tungsten or molybdenum or an alloy thereof. GB Patent 27002.
- [3] Weintraub G, Rush H (1913) Process and apparatus for sintering refractory materials. US Patent 1071488A.
- [4] Taylor GF (1933) Apparatus for Making Hard Metal Compositions. U.S. Patent 1896854.
- [5] Lenel FV (1955) Resistance Sintering Under Pressure. *Journal of Materials* 7(1):158-167.
- [6] Montes JM, Rodríguez JA, Cuevas FG, Cintas J (2011) Consolidation by Electrical Resistance Sintering of Ti Powder. *J. Mater. Sci.* 46(15):5197-5207.
- [7] Orrù R, Licheri R, Locci AM, Cincotti A, Cao G (2009) Consolidation/synthesis of materials by electric current activated/assisted sintering. *Mat. Sci. Eng. R.* 63:127-287.
- [8] Munir ZA, Quach DV, Ohyanagi M (2011) Electric current activation of sintering: a review of the pulsed electric current sintering process. *J. Am. Ceram. Soc.* 94:1-19.
- [9] Olevsky EA, Bradbury WL, Haines CD, Martin DG, Kapoor D (2012) Fundamental aspects of spark plasma sintering: I. Experimental analysis of scalability. *J. Am. Ceram. Soc.* 95:2406-2413.
- [10] Olevsky EA, Garcia-Cardona C, Bradbury WL, Haines CD, Martin DG, Kapoor D (2012) Fundamental aspects of spark plasma sintering: II. Finite element analysis of scalability. *J. Am. Ceram. Soc.* 95:2414-2422.
- [11] Montes JM, Cuevas FG, Cintas J, Urban P (2015) A One-Dimensional Model of the Electrical Resistance Sintering Process. *Met. Mater. Trans. A* 46:963-980.

- [12] MPIF Standard 45 (2002), Determination of compressibility of metal powders, in: Standard test methods for metal powders and powder metallurgy products, MPIF, Metal Powder Industries Federation, Princeton, NJ, USA.
- [13] MPIF Standard 46 (2016) Determination of tap density of metal powders, in: Standard test methods for metal powders and powder metallurgy products. MPIF, Metal Powder Industries Federation, Princeton, NJ, USA.
- [14] Secondi J (2002) Modelling powder compaction: From a pressure-density law to continuum mechanics. *Powder Metall.* 45(3):213-217.
- [15] Montes JM, Cuevas FG, Cintas J, Urban P (2012) Densification rate of metal powders during hot uniaxial compaction, *Powder Metallurgy* 55(5):388-394.
- [16] Haberman R (1987) *Elementary Applied Partial Differential Equations*. Prentice-Hall International Inc., Englewood Cliffs, NJ, USA.
- [17] *Smithells Metals Reference Book*, 8th ed. (2004) Gale WF, Totemeier TC (Eds.). Elsevier Butterworth-Heinemann Ltd, Oxford, UK.
- [18] Pierson HO (1996) *Handbook of Refractory Carbides and Nitrides: Properties, Characteristics, Processing and Applications*. Noyes Publications, Westwood, New Jersey, USA.
- [19] Kingery WD, Bowen HK, Uhlmann DR (1976) *Introduction to Ceramics*, 2nd ed. Wiley, New York, USA.
- [20] Frost HJ, Ashby MF (1982) *Deformation-mechanism maps. The plasticity and creep of metals and ceramics*. Pergamon Press, Oxford, UK.
- [21] Evans UR (1968) *The corrosion and oxidation of metals: first supplementary volume*. Edward Arnold Ltd., London, UK.
- [22] Tsuda N, Nasu K, Fujimori A, Siratori K (2000) *Electronic Conduction in Oxides*, 2nd ed. Springer-Verlag, Berlin, Germany.